

Radiative ${}^3\text{He}(\alpha, \gamma){}^7\text{Be}$ reaction in Halo Effective Field Theory

Renato Higa ^{a,*} Gautam Rupak ^{b,†} and Akshay Vaghani ^{b,‡}

^a *Instituto de Física, Universidade de São Paulo,*

R. do Matão 1371, 05508-090, São Paulo, SP, Brazil

^b *Department of Physics & Astronomy and HPC² Center for Computational Sciences,*

Mississippi State University, Mississippi State, MS 39762, U.S.A.

Abstract

In this work we study the radiative capture of ${}^3\text{He}$ on ${}^4\text{He}$ within the halo effective field theory framework. At leading order the capture amplitude comprises the initial state s -wave strong and Coulomb interactions summed to all orders, and depends on four parameters that can, in principle, be extracted from elastic ${}^3\text{He}$ - α scattering alone. At next-to-leading order, s - to p -wave initial state radiation with non-perturbative Coulomb and two-body currents contribute, with two extra parameters from the latter that are fitted to capture data. We perform three different fits of our parameters to available scattering data and most recent capture data. Our astrophysical S -factor, $S_{34} \sim 0.60 \text{ keV} \cdot \text{b}$, is slightly above the average in the literature, though consistent within current error bars.

PACS numbers: 25.40.Lw, 25.20.-x

Keywords: radiative capture, halo nuclei, effective field theory

* higa@if.usp.br

† grupak@u.washington.edu

‡ av298@msstate.edu

I. INTRODUCTION

Low-energy reaction rates involving light nuclei became a recurrent subject nowadays, given their importance in many astrophysical processes. As astronomical observations aim at more accuracy, comparable improvements from experiments and theoretical estimates are called for these reactions. An example is the process ${}^3\text{He}(\alpha, \gamma){}^7\text{Be}$ that takes place in the interior of our Sun. The astrophysical S -factor for this reaction within the Gamov window $E_G \sim 20$ keV is the main source of uncertainty in the solar neutrino flux detected on Earth. For instance, the flux of neutrinos from the β^+ decay of ${}^8\text{B}$ and from the electron capture on ${}^7\text{Be}$ are proportional to $S_{34}^{0.81}$ and $S_{34}^{0.86}$, respectively [1–3]. The first weak decay provides energetic solar neutrinos that were detected by Super-K [4] and SNO [5] but depends also on the ${}^7\text{Be}(p, \gamma){}^8\text{B}$ reaction rate. Electron capture on ${}^7\text{Be}$, on the other hand, provides a solar neutrino flux three orders of magnitude higher than the former process [6, 7], with less energetic neutrinos possible to be measured by the BOREXINO experiment at Gran Sasso [8], and depends exclusively on the ${}^3\text{He}(\alpha, \gamma){}^7\text{Be}$ reaction. In either case, the need for a better description of the latter at very low energies is of prime importance in order to improve potential constraints from solar neutrinos, like mass hierarchy, flavor mixing angles and CP violating phases. Besides neutrino physics, the ${}^3\text{He}(\alpha, \gamma){}^7\text{Be}(e^-, \nu){}^7\text{Li}$ chain reaction is the main source of ${}^7\text{Li}$ production during big bang nucleosynthesis (BBN), with a Gamov window $100 \text{ keV} \lesssim E_G \lesssim 900 \text{ keV}$. The primordial abundance of ${}^7\text{Li}$ calculated from BBN and WMAP cosmic baryon density measurements is a factor of 3 to 4 times larger than observations of metal-poor stars in our galaxy [1, 9, 10], which constitutes the so-called lithium problem. Many proposals to solve this puzzle, that involves alternative astronomical measurements and modeling, nuclear, and particle physics, can be strongly constrained with more reliable information on S_{34} , since the abundance ratio ${}^7\text{Li}/\text{H} \propto S_{34}^{0.96}$ [1, 9].

Given its importance to the topics mentioned above, several measurements of the ${}^3\text{He}(\alpha, \gamma){}^7\text{Be}$ reaction were done in the past (see [3] and references therein) and most recent years [1, 11]. As pointed out in [1], measurements done prior to the review [3] fall into two discrepant groups—those based on induced ${}^7\text{Be}$ activity, and those relying on prompt γ -ray detection. Due to improvements in detectors and background suppressions, this discrepancy is no longer present in the most recent measurements [11]. Nevertheless, error bars are still relatively large in the low-energy regime of astrophysical interest, due to

the strong suppression of events by the Coulomb repulsion. The higher energy data where statistics are better shall therefore be theoretically extrapolated down to astrophysically relevant energies in as much less model-dependent way as possible.

The ${}^7\text{Be}$ nucleus has a predominant ${}^3\text{He}\text{-}\alpha$ cluster structure. Its ground state binding energy, $B_0 \sim 1.6$ MeV, is considerably smaller than the proton separation energy in ${}^3\text{He}$ ($S_p \sim 5.5$ MeV) and the energy of the first excited state of the α particle (~ 20 MeV). The distinct two-cluster configuration of ${}^7\text{Be}$, with tight constituents and the low-energy regime one is interested in, make this reaction very suitable for a halo effective field theory (halo EFT) approach. Halo EFT was first formulated in Refs. [12, 13] in their study of the shallow p -wave neutron-alpha resonance and applied to other systems, such as the s -wave alpha-alpha resonance [14, 15], three-body halo nuclei [16, 17], coupled-channel proton- ${}^7\text{Li}$ scattering [18], electromagnetic transitions [19] and capture reactions [20–26]. In this work, we apply the same ideas to the ${}^3\text{He}(\alpha, \gamma){}^7\text{Be}$ radiative reaction, following a two-cluster approach of point-like objects at leading order (LO) approximation. Corrections due to the structure of each cluster and higher order electromagnetic interactions are taken into account in perturbation theory. In halo EFT, therefore, a systematic and model-independent expansion of observables is achieved through the use of an expansion parameter —formed by the ratio of a soft momentum scale Q , associated with the shallowness of the binding of the clusters, and a hard momentum scale Λ , related to the tightness of the cores. Moreover, the formalism guarantees unambiguous inclusion of electromagnetic interactions that preserve the required symmetry constraints, such as gauge invariance. In this study we find that the LO process, given by the sum of initial strong interactions to all orders with intermediate one-body current radiation, provides nearly all of the radiative capture contribution. The LO term depends on four low-energy constants that can be determined, in principle, from the ${}^3\text{He}\text{-}\alpha$ elastic scattering alone. A better partial wave analysis of this elastic process with reduced uncertainties would therefore put stronger constraints on the radiative capture. Next-to-leading order (NLO) corrections come from the initial state radiation and electromagnetic two-body currents, this latter bringing two extra low-energy parameters that are fit to capture data. Our S -factor values are consistent with other determinations within error bars, though with a slightly higher mean value.

The paper is organized as follows. In Sec. II we briefly comment on the energy scales, degrees of freedom, and channels relevant to the dominant E1 transition, as well as the

construction of the corresponding interaction lagrangian. Sec. III presents the main elements necessary to deal with Coulomb interactions between the ${}^3\text{He}$ and α nuclei. Elastic scattering for both physical initial state and bound final state interactions are obtained in the halo EFT framework in Sec. IV. There we also relate the EFT couplings to the effective range parameters and set the power counting. Sec. V collects the relevant expressions of the EFT capture amplitude and cross section, whose numerical results are shown and discussed in Sec. VI. Our concluding remarks are presented in Sec. VII.

II. INTERACTION

The halo EFT we construct treats the ${}^7\text{Be}$ nucleus as a bound state of point-like nuclear clusters ${}^3\text{He}$ and α . The $\frac{3}{2}^-$ ground state has a binding energy $B_0 = 1.5866$ MeV, and the $\frac{1}{2}^-$ first excited state has a binding energy $B_1 = 1.1575$ MeV. The next excited state of ${}^7\text{Be}$ is about 3 MeV above the ${}^3\text{He}$ - α threshold [27]. In halo EFT the ground and first excited states are included respectively as ${}^2P_{3/2}$ and ${}^2P_{1/2}$ in the spectroscopic notation ${}^{2S+1}L_J$. The states beyond the first excited states are not included in the low-energy theory. Similarly, only the ground states of ${}^3\text{He}$ and α are relevant at astrophysical energies.

Early works on radiative capture ${}^3\text{He}(\alpha, \gamma){}^7\text{Be}$ indicate it is dominated by E1 transition from initial s -wave state at low energies. Thus we consider the following Lagrangian for the calculation,

$$\begin{aligned} \mathcal{L} = & \psi^\dagger \left[i\partial_0 + \frac{\nabla^2}{2m_\psi} \right] \psi + \phi^\dagger \left[i\partial_0 + \frac{\nabla^2}{2m_\phi} \right] \phi \\ & + \chi_{[j]}^{(\zeta)\dagger} \left[\Delta^{(\zeta)} + i\partial_0 + \frac{\nabla^2}{2M} \right] \chi_{[j]}^{(\zeta)} + h^{(\zeta)} \left[\chi_{[j]}^{(\zeta)\dagger} \psi P_{[j]}^{(\zeta)} \phi + \text{h. c.} \right], \end{aligned} \quad (1)$$

where the spin-1/2 fermion field ψ represents the $\frac{1}{2}^+ {}^3\text{He}$ nucleus field with mass $m_\psi = 2809.41$ MeV, and the scalar field ϕ represents the spinless $0^+ \alpha$ field, with mass $m_\phi = 3728.4$ MeV. $M = m_\psi + m_\phi$ is the total mass. We use natural units with $\hbar = 1 = c$. Note, in the intermediate steps, we display more significant digits than appropriate given theory and fitting errors, in the final result. The projectors $P_{[j]}$ and the auxiliary fields $\chi_{[j]}^{(\zeta)}$ carry vector and spinor indices $[j]$ to specify the relevant spin-angular momentum channels for the incoming state $\zeta = {}^2S_{1/2}$, final ground state $\zeta = {}^2P_{3/2}$, and final excited state $\zeta = {}^2P_{1/2}$, described below.

The s -wave interaction can be written using a spin-1/2 auxiliary field $\chi^{\alpha,s}$ as:

$$\chi^{\alpha,s\dagger} \left[\Delta^{(s)} + i\partial_0 + \frac{\nabla^2}{2M} \right] \chi^{\alpha,s} + h^{(s)} [\chi^{\alpha,s\dagger} P^{\alpha\beta,s} \psi^\beta \phi + \text{h.c.}] , \quad (2)$$

where the spinor indices α, β on the fields $\chi^{\alpha,s}$ and ψ^β are contracted using the diagonal s -wave projector $P^{\alpha\beta,s} = \delta^{\alpha\beta}$. The spinor index $\alpha = 1, 2$. The two s -wave couplings $\Delta^{(s)}$ and $h^{(s)}$ can be fitted to scattering length a_0 and effective range r_0 for elastic scattering of ^3He and α . We discuss this in more detail when we consider the relevant power counting.

For the final state, we want to project the vector index $i = 1, 2, 3$ for the p -wave and the spinor index α for the ^3He spin into total angular momentum $j = 1/2$ and $j = 3/2$ pieces. This can be done for a generic auxiliary field χ_i^α as follows:

$$\chi_i^\alpha = \frac{1}{3}(\sigma_i \sigma_j)^{\alpha\beta} \chi_j^\beta + \left[\delta_{ij} \delta^{\alpha\beta} - \frac{1}{3}(\sigma_i \sigma_j)^{\alpha\beta} \right] \chi_j^\beta, \quad (3)$$

where the two pieces are the irreducible forms representing the $^2P_{1/2}$ and $^2P_{3/2}$ channels respectively. The Pauli matrices σ_i 's act on the spinor indices. The two p -wave interactions can then be written as

$$\chi_i^{\alpha,\zeta\dagger} \left[\Delta^{(\zeta)} + i\partial_0 + \frac{\nabla^2}{2M} \right] \chi_i^{\alpha,\zeta} + \sqrt{3} h^{(\zeta)} \left[\chi_i^{\alpha,\zeta\dagger} P_{ij}^{\alpha\beta,\zeta} \psi^\beta \left(\frac{\vec{\nabla}}{m_\phi} - \frac{\overleftarrow{\nabla}}{m_\psi} \right)_k \phi + \text{h.c.} \right], \quad (4)$$

where the p -wave projectors are

$$P_{ij}^{\alpha\beta,\zeta} = \frac{1}{3}(\sigma_i \sigma_j)^{\alpha\beta} \quad \text{for } \zeta = ^2P_{1/2}, \quad (5)$$

and $P_{ij}^{\alpha\beta,\zeta} = \delta_{ij} \delta^{\alpha\beta} - \frac{1}{3}(\sigma_i \sigma_j)^{\alpha\beta} \quad \text{for } \zeta = ^2P_{3/2}.$

The two couplings $\Delta^{(\zeta)}, h^{(\zeta)}$ in each of the two p -wave channels can be determined from the corresponding binding momentum and effective range. For bound states, both of these couplings contribute at leading order [12, 13]. This remains true even in the presence of long-range Coulomb interaction as we have here.

The capture calculation proceeds through E1 transition. At LO, we couple the external photon through minimal substitution, that corresponds to gauging the momentum of the charged particle, $\mathbf{p} \rightarrow \mathbf{p} + Ze\mathbf{A}$, where Z is the charge number. $Z = 2$ for both the ^3He and α nuclei. We include the long-range Coulomb interaction between the ^3He and α nuclei to all orders in perturbation by summing the Coulomb ladder as described below. At NLO, two-body currents that are not related to elastic scattering operators by gauge invariance

contribute. Two-body currents that contribute to E1 transition between s -wave, and p -wave ground and excited states can be written using the auxiliary fields as

$$eL_{E1}^{(\zeta)}\sqrt{3}h^{(s)}h^{(\zeta)}\chi_i^{\alpha,\zeta\dagger}P_{ij}^{\alpha\beta,\zeta}\chi_j^{\beta,s}E_j. \quad (6)$$

We include factors of $h^{(s)}$, $h^{(\zeta)}$ in the definition of the coupling L_{E1} for convenience. In the absence of Coulomb interaction this reduces to a factor of $2\pi/(\mu\sqrt{r_0r_1^{(\zeta)}})$ that has been suggested earlier [28].

III. COULOMB LADDER

For scattering of two charged particles ${}^3\text{He}$ and α at low energy, the relevant quantity that provides the strength of Coulomb photon exchanges is the Sommerfeld parameter $\eta_p = \alpha_e Z_\psi Z_\phi \mu / p$, where Z_ψ and Z_ϕ are the charge number of ${}^3\text{He}$ and α , respectively, $\alpha_e = e^2/(4\pi) \sim 1/137$ is the electromagnetic fine structure constant, μ is the reduced mass, and p is the relative center-of-mass (c.m.) momentum. The inverse of the Bohr radius of the system defines the momentum scale $k_C = \alpha_e Z_\psi Z_\phi \mu$ and the Sommerfeld parameter is written as the ratio $\eta_p = k_C/p$. Each photon exchange is proportional to η_p . In the high-energy side where $p \gg k_C$ photon exchanges can be treated in perturbation theory. However, in the low momentum region that we are interested in, $p \lesssim k_C$, multiple photon exchanges contribute at least at the same order, forcing the summation of Coulomb ladder diagrams, Fig. 1.

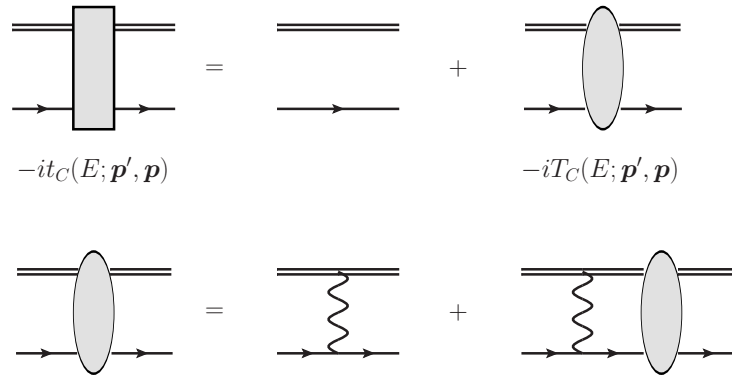


FIG. 1. Coulomb ladder diagrams. The double line represents the scalar α particle, and the single line with an arrow the fermionic ${}^3\text{He}$ nucleus. The wavy lines represent photons. We only include Coulomb photon interaction between the charged particles.

The Coulomb scattering amplitude T_C satisfies the following useful relations

$$\begin{aligned} |\chi_p^{(\pm)}\rangle &= |\mathbf{p}\rangle + \hat{G}_0^{(\pm)} \hat{T}_C |\mathbf{p}\rangle, \\ \hat{G}_C^{(\pm)} &= \hat{G}_0^{(\pm)} + \hat{G}_0^{(\pm)} \hat{T}_C \hat{G}_0^{(\pm)}, \end{aligned} \quad (7)$$

where $|\mathbf{p}\rangle$ is a plane wave state in the two-particle center-of-mass (c.m.) system and $|\chi_k^{(+)}\rangle$ ($|\chi_k^{(-)}\rangle$) is the incoming (outgoing) Coulomb scattering state. The free and Coulomb Green's functions as operators are respectively written as

$$\hat{G}_0^{(\pm)} = (E - \hat{H}_0 \pm i\epsilon)^{-1} \quad \text{and} \quad \hat{G}_C^{(\pm)} = (E - \hat{H}_0 - \hat{V}_C \pm i\epsilon)^{-1}. \quad (8)$$

The $\pm i\epsilon$ sign in the definitions correspond to retarded and advanced Green's functions. Taking expectation values between final $\langle \mathbf{p}' |$ and initial $|\mathbf{p}\rangle$ momentum states, one can derive several useful relations,

$$\begin{aligned} G_0^{(\pm)}(E; \mathbf{p}', \mathbf{p}) &\equiv \langle \mathbf{p}' | \hat{G}_0^{(\pm)} | \mathbf{p} \rangle = \frac{(2\pi)^3 \delta(\mathbf{p}' - \mathbf{p})}{E - p'^2/(2\mu) \pm i\epsilon}, \\ \frac{T_C(E; \mathbf{p}', \mathbf{p})}{E - p'^2/(2\mu) \pm i\epsilon} &\equiv \langle \mathbf{p}' | \hat{G}_0 \hat{T}_C | \mathbf{p} \rangle = \chi_p^{(\pm)}(\mathbf{p}') - (2\pi)^3 \delta(\mathbf{p}' - \mathbf{p}), \\ G_C^{(\pm)}(E; \mathbf{p}', \mathbf{p}) &\equiv \langle \mathbf{p}' | \hat{G}_C^{(\pm)} | \mathbf{p} \rangle = G_0^{(\pm)}(E; \mathbf{p}', \mathbf{p}) + \frac{T_C(E; \mathbf{p}', \mathbf{p})}{[E - p'^2/(2\mu) \pm i\epsilon][E - p^2/(2\mu) \pm i\epsilon]}, \end{aligned} \quad (9)$$

with $\chi_p^{(\pm)}(\mathbf{p}') \equiv \langle \mathbf{p}' | \chi_p^{(\pm)} \rangle$. The diagrammatic relation between \hat{t}_C and \hat{T}_C from Fig. 1 can be expressed as

$$t_C(E; \mathbf{p}', \mathbf{p}) = (2\pi)^3 \delta(\mathbf{p}' - \mathbf{p}) \left(E - \frac{p'^2}{2\mu} \pm i\epsilon \right) + T_C(E; \mathbf{p}', \mathbf{p}), \quad (10)$$

and helps write $t_C(E; \mathbf{p}', \mathbf{p})$ in terms of $\chi_p^{(\pm)}(\mathbf{p}')$ and $G_C^{(\pm)}(E; \mathbf{p}', \mathbf{p})$.

The Coulomb wave function and the retarded Green's function are known in closed form in coordinate space [29, 30],

$$\begin{aligned} \tilde{\chi}_p^{(\pm)}(\mathbf{r}) &\equiv e^{-\frac{\eta_p \pi}{2}} \Gamma(1 \pm i\eta_p) {}_1F_1(\mp i\eta_p, 1; \pm i p r - i \mathbf{p} \cdot \mathbf{r}) e^{i \mathbf{p} \cdot \mathbf{r}}, \\ &= \sum_{l=0}^{\infty} (2l+1) i^l e^{i\sigma_l} P_l(\hat{\mathbf{r}} \cdot \hat{\mathbf{r}}') \frac{F_l(\eta_p, pr)}{pr}, \\ G_C^{(+)}(E; \mathbf{r}', \mathbf{r}) &\equiv \sum_{l=0}^{\infty} (2l+1) P_l(\hat{\mathbf{r}} \cdot \hat{\mathbf{r}}') G_C^{(l)}(E, r', r), \\ G_C^{(l)}(E, r', r) &= -\frac{i\mu p}{2\pi} \frac{F_l(\eta_p, r'p)}{r'p} \frac{F_l(\eta_p, rp)}{rp}, \end{aligned} \quad (11)$$

where

$$\begin{aligned}
F_l(\eta_p, \rho) &= C_l(\eta_p) \rho^{l+1} e^{-i\rho} M(l+1-i\eta_p, 2l+2, +2i\rho), \\
H_l^{(+)}(\eta_p, \rho) &= (-i)^l e^{\pi\eta_p/2} \sqrt{\frac{\Gamma(l+1+i\eta_p)}{\Gamma(l+1-i\eta_p)}} W_{-i\eta_p, l+1/2}(-i2\rho), \\
C_l(\eta_p) &= \frac{2^l e^{-\pi\eta_p/2} |\Gamma(l+1+i\eta_p)|}{\Gamma(2l+2)},
\end{aligned} \tag{12}$$

with conventionally defined Kummer $M(a, b, z)$ and the Whittaker $W_{k, \mu}(z)$ functions. $F_l(\eta_p, \rho)$ is the regular Coulomb wave function, the irregular wave function is given by $G_l(\eta_p, \rho) = H_l^{(+)}(\eta_p, \rho) - iF_l(\eta_p, \rho)$, and $\sigma_l = \arg \Gamma(l+1+i\eta_p)$ is the Coulomb phase shift. We define the Coulomb Green's function for a bound state with binding energy B as

$$G_C^{(l)}(-B, r', r) = -i \frac{\mu\gamma}{2\pi} \frac{F_l(\eta_{i\gamma}, i\gamma r')}{i\gamma r'} \frac{H_l^{(+)}(\eta_{i\gamma}, i\gamma r)}{i\gamma r}, \tag{13}$$

where $\gamma = \sqrt{2\mu B}$ is the binding momentum. The coordinate space definitions assume $r' < r$, In the limit $r' \sim 0 \ll r \sim \infty$ for charged neutral particles ($Z_\psi = 0 = Z_\phi$), we recover the expected result

$$G_C^{(0)}(-B, r' \rightarrow 0, r) \sim -\frac{\mu}{2\pi r} e^{-\gamma r}. \tag{14}$$

IV. ELASTIC SCATTERING

The elastic scattering amplitude $T(E; \mathbf{p}', \mathbf{p})$ in the presence of both short-range strong and long-range Coulomb interaction is traditionally written as

$$T(E; \mathbf{p}', \mathbf{p}) = T_C(E; \mathbf{p}', \mathbf{p}) + T_{SC}(E; \mathbf{p}', \mathbf{p}), \tag{15}$$

where the purely Coulomb contribution can be written as

$$T_C(E; \mathbf{p}', \mathbf{p}) = \sum_{l=0}^{\infty} (2l+1) T_C^{(l)}(E; p) P_l(\hat{\mathbf{p}} \cdot \hat{\mathbf{p}}') = -\frac{2\pi}{\mu} \sum_{l=0}^{\infty} (2l+1) \frac{e^{2i\sigma_l} - 1}{2ip} P_l(\hat{\mathbf{p}} \cdot \hat{\mathbf{p}}'), \tag{16}$$

using the incoming (outgoing) c.m. momentum \mathbf{p} (\mathbf{p}').

The on-shell Coulomb subtracted amplitude can also be expanded in partial waves as

$$T_{SC}^{(l)} = -\frac{2\pi}{\mu} \frac{e^{2i\sigma_l}}{p \cot \delta_l - ip}, \tag{17}$$

where the full phase shift is simply $\delta_l + \sigma_l$. The Coulomb subtracted phase shift is usually expressed in terms of a modified effective range expansion

$$\left[\frac{\Gamma(2l+2)}{2^l \Gamma(l+1)} \right]^2 [C_l(\eta_p)]^2 p^{2l+1} (\cot \delta_l - i) = -\frac{1}{a_l} + \frac{1}{2} r_l p^2 - \frac{2k_C p^{2l}}{\Gamma(l+1)^2} \frac{|\Gamma(l+1+i\eta_p)|^2}{|\Gamma(1+i\eta_p)|^2} H(\eta_p), \quad (18)$$

$$H(\eta) = \psi(i\eta) + \frac{1}{2i\eta} - \ln(i\eta),$$

with $\psi(x)$ the digamma function.

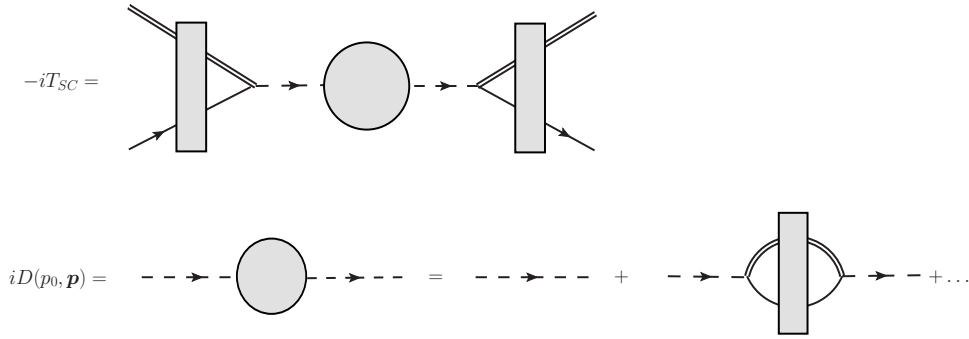


FIG. 2. Elastic scattering in s - and p -wave. The dashed line represent the auxiliary field χ in s - and p -wave as appropriate. Rest of the notations is the same as in Fig. 1.

The amplitude T_{SC} is given in EFT by the set of diagrams in Fig. 2. The s -wave amplitude for c.m. incoming momentum \mathbf{p} and outgoing momentum \mathbf{p}' with $p = |\mathbf{p}| = |\mathbf{p}'|$ and $E = p^2/(2\mu)$ can be written as

$$\begin{aligned} -iT_{SC}^{(l=0)} &= (2\mu)^2 \left[\int \frac{d^3k}{(2\pi)^3} \frac{t_c(E; \mathbf{p}', \mathbf{k})}{k^2 - p^2 - i\epsilon} \right] [-i(h^{(s)})^2 D^{(s)}(E, 0)] \left[\int \frac{d^3l}{(2\pi)^3} \frac{t_c(E; \mathbf{l}, \mathbf{p})}{l^2 - p^2 - i\epsilon} \right] \quad (19) \\ &= -i[h^{(s)}]^2 D^{(s)}(E, 0) \tilde{\chi}_{p'}^{(-)*}(0) \tilde{\chi}_p^{(+)}(0) = -i[h^{(s)}]^2 D^{(s)}(E, 0) C_0^2(\eta_p) e^{i2\sigma_0}, \end{aligned}$$

where the dressed dimer propagator is given by

$$D^{(s)}(p_0, \mathbf{p} = 0) = \frac{1}{\Delta^{(s)} + p_0 - [h^{(s)}]^2 J_0(\sqrt{2\mu p_0})}, \quad (20)$$

$$J_0(\sqrt{2\mu E}) = J_0(p) = G_C(E; r=0, r'=0) = -2\mu \int \frac{d^3q}{(2\pi)^3} \frac{1}{[q^2 - p^2 - i\epsilon]} \frac{2\pi\eta_q}{[e^{2\pi\eta_q} - 1]}.$$

Comparing the modified ERE in Eq. (18) to the s -wave EFT expression, we can determine

the two couplings in terms of a_0 and r_0 ,

$$\Delta^{(s)} = \frac{\mu h^{(s)2}}{2\pi a_0} - \frac{\mu h^{(s)2}}{2\pi} \left\{ 2k_C \left[\frac{1}{D-4} - \ln \left(\frac{\lambda\sqrt{\pi}}{2k_C} \right) - 1 + \frac{3}{2}C_E \right] + \lambda \right\}, \quad (21)$$

$$[h^{(s)}]^2 = -\frac{2\pi}{\mu^2 r_0},$$

where $D \rightarrow 4$ and λ is the renormalization scale within the power-divergence subtraction (PDS) scheme. The elastic scattering amplitude requires non-perturbative treatment of the Coulomb photons at low energies. However, it is not clear if the short-range interaction contained in the parameters a_0 , r_0 , etc., should be included in perturbation or not. Fitting the EFT expression to both elastic and capture data later, we find that both the scattering length a_0 and the effective range r_0 contribute at leading order. We propose a power counting where $a_0 \sim \Lambda/Q^2$ is fine tuned and $r_0 \sim 1/\Lambda$ is of natural size, which is very similar to the s -wave α - α scattering [14]. Then the s -wave scattering amplitude gets LO contributions from a_0 , r_0 for small momenta $p \sim Q$, and the contribution from a natural sized shape parameter $s_0 \sim 1/\Lambda^3$, is suppressed by factors of Q^2/Λ^2 . This is the largest source of theory error in the calculation.

The p -wave amplitude is written as

$$-iT_{SC}^{(1)} = -i[h^{(\zeta)}]^2 D^{(\zeta)}(E, 0) [\nabla_a \tilde{\chi}_p^{(-)*}(0)] [\nabla_a \tilde{\chi}_p^{(+)}(0)], \quad (22)$$

with the p -wave dressed dimer propagator written as

$$D^{(\zeta)}(E, 0) = \frac{1}{\Delta^{(\zeta)} + E - 3[h^{(\zeta)}]^2 J_1(p)}, \quad (23)$$

$$J_1(p) = -\frac{2\mu}{n} \int \frac{d^n k}{(2\pi)^n} \frac{1}{k^2 - p^2 - i\delta} [\nabla_a \tilde{\chi}_k^{(+)*}(0)] [\nabla_a \tilde{\chi}_k^{(+)}(0)].$$

$J_1(p)$ is given by a divergent integral that we regulate through dimensional regularization in n space dimensions. Using the relations

$$[\nabla_a \tilde{\chi}_p^{(-)*}(0)] [\nabla_a \tilde{\chi}_k^{(+)}(0)] = e^{-\pi\eta_p} \Gamma(2 + i\eta_p)^2 \mathbf{p}' \cdot \mathbf{p}, \quad (24)$$

$$[\nabla_a \tilde{\psi}_k^{(+)*}(0)] [\nabla_a \tilde{\psi}_k^{(+)}(0)] = (k^2 + \beta^2) \frac{2\pi\eta_k}{e^{2\pi\eta_k} - 1},$$

the PDS prescription for the integrals, and Eq. (18), one gets

$$\begin{aligned}\Delta^{(\zeta)} &= \frac{h^{(\zeta)2}}{2\pi\mu a_1} - \frac{h^{(\zeta)2}}{2\pi\mu} \left\{ 2k_C^3 \left[\frac{1}{D-4} - \ln \left(\frac{\lambda\sqrt{\pi}}{2k_C} \right) - 1 + \frac{3}{2}C_E \right] \right. \\ &\quad \left. + k_C^2 \left(\frac{3\lambda}{2} - \frac{2k_C}{3} \right) + 8\pi^2 k_C^3 \zeta'(-2) + \frac{\pi^2 \lambda k_C^2}{2} - \frac{3\pi \lambda^2 k_C}{2} + \frac{\pi \lambda^3}{2} \right\}, \\ \frac{1}{[h^{(\zeta)}]^2} &= -\frac{r_1}{2\pi} - \frac{1}{\pi} \left\{ 2k_C \left[\frac{1}{D-4} - \ln \left(\frac{\lambda\sqrt{\pi}}{2k_C} \right) - 1 + \frac{3}{2}C_E \right] + \left(\frac{3\lambda}{2} - \frac{2k_C}{3} \right) \right\}.\end{aligned}\quad (25)$$

The dressed p -wave dimer propagator defines the wave-function renormalization constant via

$$\frac{1}{\mathcal{Z}^{(\zeta)}} = \frac{\partial}{\partial p_0} [D^{(\zeta)}(p_0; \mathbf{p})^{-1}] \big|_{p_0=p^2/(2\mu)-B^{(\zeta)}}, \quad (26)$$

where $B^{(\zeta)}$ is the p -wave binding energy. Straightforward calculation leads to

$$-\frac{2\pi}{h^{(\zeta)2}\mathcal{Z}^{(\zeta)}} = r_1^{(\zeta)} - 4k_C H\left(-i\frac{k_C}{\gamma}\right) - \frac{2k_C^2}{\gamma^3}(k_C^2 - \gamma^2) \left[\psi'\left(\frac{k_C}{\gamma}\right) - \frac{\gamma^2}{2k_C^2} - \frac{\gamma}{k_C} \right]. \quad (27)$$

V. RADIATIVE CAPTURE

We assign the c.m. momenta \mathbf{p} to the α particle, and \mathbf{k} to the outgoing photon in the final state. From energy-momentum conservation $|\mathbf{k}| = (p^2 + \gamma^2)/(2\mu) \sim Q^2/\mu \ll Q \sim \gamma \sim p$ in the EFT power counting. Thus in a typical loop-calculation a combination such as $E_\psi + k_0 + q_0 - (\mathbf{q} + \mathbf{k} + \mathbf{p})^2/(2m_\psi)$ is approximated as $E_\psi + k_0 - (\mathbf{q} + \mathbf{p})^2/(2m_\psi) \sim Q^2/\mu$ where $E_\psi = p^2/(2m_\psi)$ and (q_0, \mathbf{q}) is the loop energy-momentum. This approximation corresponds to zero-recoil of the final bound state ${}^7\text{Be}$. We count $Q/\mu \ll Q/\Lambda$ and neglect recoil effects in this calculation up to NLO.

In this section we present some of the Feynman diagrams that contribute to the capture process, see Figs. 3, 4, 5. In the next section when we present our analysis, we elaborate more on the power counting and discuss how these set of diagrams constitutes the EFT contribution up to NLO. We consider E1 transitions from the initial ${}^2S_{1/2}$ state to both final bound states, ground ${}^2P_{3/2}$ and excited ${}^2P_{1/2}$. The external photon is minimally coupled to the charged clusters at LO.

The first set of diagrams only include Coulomb interactions for the incoming charged

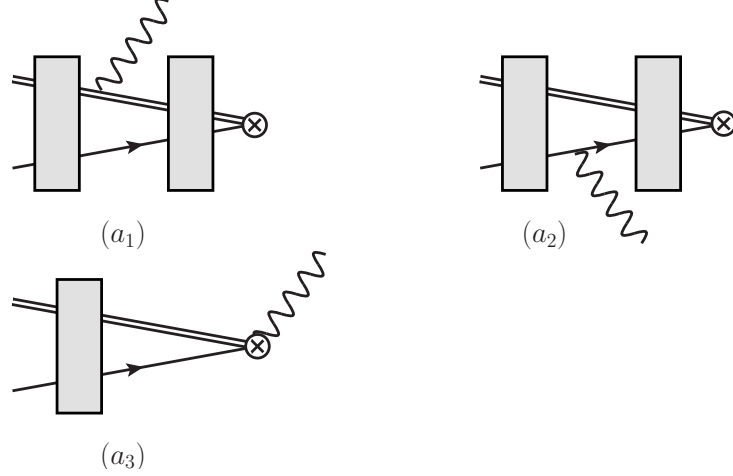


FIG. 3. Group A diagrams. Radiative capture without initial state strong interaction. The \otimes represents the final bound state. The external photon represented by the wavy line is minimally coupled to the charged particles as described in the text. The rest of the notation is same as in Figs 1, 2.

particles ${}^3\text{He}$ and α . We find

$$\begin{aligned}
 (a_1) + (a_2) &= -\frac{e^{i\sigma_0} A(p)}{\mu} \Gamma_{aa}^{(\zeta)}, \\
 (a_3) &= -\tilde{\chi}_p^{(+)}(\mathbf{r} = \mathbf{0}) \Gamma_{aa}^{(\zeta)} = -C_0(\eta_p) e^{i\sigma_0} \Gamma_{aa}^{(\zeta)}, \\
 A(p) &= \frac{2\gamma\mu}{3} \Gamma(2 + k_C/\gamma) \int_0^\infty dr \, r W_{-k_C/\gamma, 3/2}(2\gamma r) \partial_r \left[\frac{F_0(k_C/p)}{pr} \right],
 \end{aligned} \tag{28}$$

where the index ζ refers to the final state p -wave bound states. The corresponding binding momentum γ is given by $\gamma_0 = \sqrt{2\mu B_0}$ and $\gamma_1 = \sqrt{2\mu B_1}$ for the ground and the first excited states, respectively. The Whittaker function $W_{-k_C/\gamma, 3/2}(2\gamma r)$ is associated with the final p -wave bound state, and the s -wave Coulomb wave function $F_0(\eta_p)$ is associated with the initial incoming scattering state.

The projection onto the p -wave states is given by

$$\Gamma_{ab}^{(\zeta)} = \left(\frac{eZ_\phi}{m_\phi} - \frac{eZ_\psi}{m_\psi} \right) (h^{(\zeta)} \sqrt{3} \sqrt{\mathcal{Z}^{(\zeta)}} \sqrt{2m_\phi}) \epsilon_a^* U_i^{\alpha, \zeta}(-\vec{k}) P_{ib}^{\alpha\beta, \zeta} U^{\beta, \psi}(-\vec{p}), \tag{29}$$

where ϵ_a is the photon polarization vector, $\mathcal{Z}^{(\zeta)}$ is given by Eq. (27), U^ζ is the spinor field for the p -wave final state with mass $M = m_\psi + m_\phi$, and U^ψ is the spinor field for the incoming

^3He nucleus. The spinor fields satisfy the completeness relations

$$\begin{aligned} U_i^{\alpha,\zeta}(\mathbf{p})[U_j^{\beta,\zeta}(\mathbf{p})]^* &= 2MP_{ij}^{\alpha\beta,\zeta}, \\ U^{\alpha,\psi}(\mathbf{p})[U^{\beta,\psi}(\mathbf{p})]^* &= 2m_\psi\delta^{\alpha\beta}, \end{aligned} \quad (30)$$

where i, j are vector indices, and α, β are spin indices.

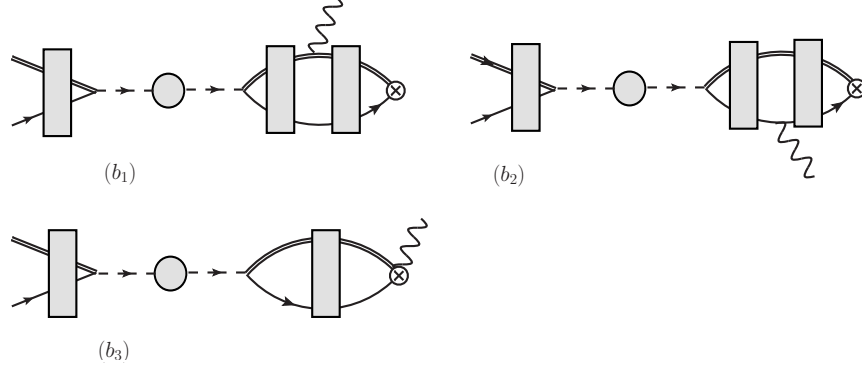


FIG. 4. Group B diagrams. Radiative capture with initial state s -wave strong interaction represented by the dressed dimer. We use the same notation as Figs. 1, 2 and 3.

The second set of diagrams from Fig. 4 involve initial state short-range interaction that is constrained by the s -wave phase shift through the ERE. We find

$$\begin{aligned} (b_1) + (b_2) &= \frac{2\pi}{\mu} \frac{C_0(\eta_p)e^{i\sigma_0}}{-\frac{1}{a_0} + r_0p^2/2 - 2k_C H(\eta_p)} \frac{B_{ab}(p)}{\mu} \Gamma_{ab}, \\ B_{ab}(p) &= 3 \int d^3r \frac{\partial G_C^{(+)}(E; 0, \mathbf{r})}{\partial r_a} \frac{r_b}{r} \left[\frac{G_C^{(1)}(-B; r, r')}{r'} \right] \Big|_{r'=0}, \\ \left[\frac{G_C^{(1)}(-B; r, r')}{r'} \right] \Big|_{r'=0} &= -\frac{\mu\gamma}{6\pi r} \Gamma(2 + k_C/\gamma) W_{-k_C/\gamma, 3/2}(2\gamma r), \\ G_C^{(+)}(E; 0, \mathbf{r}) &= -\frac{\mu}{2\pi r} \Gamma(1 - ik_C/p) W_{ik_C/p, 1/2}(-i2pr). \end{aligned} \quad (31)$$

The integral B_{ab} is divergent, which is rendered finite when combined with the contribution from the third diagram,

$$(b_3) = \frac{2\pi}{\mu} \frac{C_0(\eta_p)e^{i\sigma_0}}{-\frac{1}{a_0} + r_0p^2/2 - 2k_C H(\eta_p)} J_0(p) \Gamma_{aa}. \quad (32)$$

We regulate the divergences using PDS, which is most conveniently done in this calculation in momentum space. The divergences come from zero and single Coulomb photon exchanges.

Thus we analytically calculate the divergent pieces perturbatively up to $\mathcal{O}(\alpha_e)$ and calculate the rest (more than a single Coulomb photon) that is not divergent numerically:

$$\begin{aligned}
B_{ab}(p) &\equiv B_{ab}^{(0)}(p) + \alpha_e B_{ab}^{(1)}(p) + \Delta B_{ab}(p), \\
B_{ab}^{(0)} &\equiv B^{(0)}\delta_{ab} = \mu^2 \left[\frac{\lambda}{2\pi} + \frac{ip}{3\pi} - \frac{\gamma^2}{3\pi} \frac{ip + \gamma}{p^2 + \gamma^2} \right] \delta_{ab}, \\
\alpha_e B_{ab}^{(1)} &\equiv \alpha_e B^{(1)}\delta_{ab} = -\frac{k_C \mu^2}{2\pi} \left[\frac{1}{\epsilon} + \ln \frac{\pi \lambda^2}{4k_C^2} - \gamma_E - \frac{2}{3} + \ln 4\pi \right] \delta_{ab} + k_C C(p)\delta_{ab}, \\
C(p) &= \frac{\mu^2}{6\pi^2(p^2 + \gamma^2)} \int_0^1 dx \int_0^1 dy \frac{1}{\sqrt{x(1-x)}\sqrt{1-y}} \\
&\quad \times \left(xp^2 \ln \left[\frac{\pi}{4k_C^2} (-yp^2 + (1-y)\gamma^2/x - i\delta) \right] \right. \\
&\quad + p^2 \ln \left[\frac{\pi}{4k_C^2} (-yp^2 - (1-y)p^2/x - i\delta) \right] \\
&\quad + x\gamma^2 \ln \left[\frac{\pi}{4k_C^2} (y\gamma^2 + (1-y)\gamma^2/x - i\delta) \right] \\
&\quad \left. + \gamma^2 \ln \left[\frac{\pi}{4k_C^2} (y\gamma^2 - (1-y)p^2/x - i\delta) \right] \right).
\end{aligned} \tag{33}$$

The double integral $C(p)$ can be reduced further to a single integral that we evaluate numerically. The finite piece ΔB_{ab} is evaluated numerically where we use spherical symmetry to write $(r_b/r)[\partial/\partial r_a] = (r_a r_b/r^2)[\partial/\partial r] \rightarrow (\delta_{ab}/3)[\partial/\partial r]$ in the integral. Consequently, $\Delta B_{ab}(p) \equiv \Delta B(p)\delta_{ab}$.

We do a similar decomposition of $J_0(p)$ to write

$$\begin{aligned}
J_0(p) &= J_0^{(0)}(p) + \alpha_e J_0^{(1)} + \Delta J_0(p), \\
J_0^{(0)}(p) &= -\frac{\mu}{2\pi}(ip + \lambda), \\
\alpha_e J_0^{(1)} &= \frac{k_C \mu}{2\pi} \left[\frac{1}{\epsilon} + 1 - \gamma_E + i\pi + \ln \frac{\pi \lambda^2}{4p^2} \right],
\end{aligned} \tag{34}$$

and the finite piece as

$$\begin{aligned}
\Delta J_0(0) &= -2\mu \int \frac{d^n q}{(2\pi)^n} \frac{1}{q^2 - p^2 - i\delta} \left[\frac{2\pi\eta_q}{\exp(2\pi\eta_q) - 1} - 1 + \pi\eta_q \right] \\
&= \frac{i\mu p}{2\pi} + \frac{k_C \mu}{2\pi} \left[-2H(\eta_p) - 2\gamma_E - i\pi + \ln \frac{p^2}{k_C^2} \right].
\end{aligned} \tag{35}$$

Comparing Eqs. (33) and (34), we see that the divergent pieces cancel when combining diagrams $(b_1) + (b_2)$ with (b_3) .

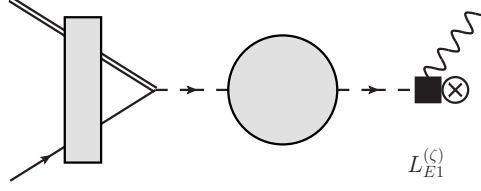


FIG. 5. Two-body current represented by the square. The rest of the notation is same as in Figs 1, 2, 3.

The third contribution is from two-body currents in Eq. (6) that contribute to E1 capture to the ground and excited states. The diagram in Fig. 5 gives the contribution

$$\frac{2\pi}{\mu} \frac{C_0(\eta_p) e^{i\sigma_0} k_0}{-1/a_0 + r_0 p^2/2 - 2k_C H(\eta_p)} \times \frac{L_{E1}^{(\zeta)}}{Z_\phi/m_\phi - Z_\psi/m_\psi} \Gamma_{aa}^{(\zeta)}. \quad (36)$$

Thus we have the following expression for the total capture amplitude

$$\begin{aligned} \mathcal{A}(p) \Gamma_{aa}^{(\zeta)} \equiv & - \left[\frac{1}{\mu} A(p) + C_0(\eta_p) - \frac{2\pi C_0(\eta_p)}{\mu^2} \frac{B^{(0)}(p) + \alpha_e B^{(1)}(p) + \Delta B(p) + \mu J_0(p)}{-\frac{1}{a_0} + r_0 p^2/2 - 2k_C H(\eta_p)} \right. \\ & \left. - \frac{2\pi}{\mu} \frac{C_0(\eta_p) k_0}{-1/a_0 + r_0 p^2/2 - 2k_C H(\eta_p)} \times \frac{L_{E1}^{(\zeta)}}{Z_\phi/m_\phi - Z_\psi/m_\psi} \right] e^{i\sigma_0} \Gamma_{aa}^{(\zeta)}. \end{aligned} \quad (37)$$

The differential cross section for capture can now be written as

$$\frac{d\sigma}{d\cos\theta} = \frac{1}{32\pi M^2} \frac{k}{p} \frac{1}{2} \left[|M^{(^2P_{1/2})}|^2 + |M^{(^2P_{3/2})}|^2 \right], \quad (38)$$

where we summed over the photon polarization in the final state and average over initial ^3He spins. The amplitude squared is

$$|M^{(\zeta)}|^2 = (2J+1) \left(\frac{Z_\phi m_\psi}{M} - \frac{Z_\psi m_\phi}{M} \right)^2 \frac{64\pi\alpha_e M^2 ([h^{(\zeta)}]^2 \mathcal{Z}^{(\zeta)})}{\mu} |\mathcal{A}(p)|^2, \quad (39)$$

with angular momentum $J = 1/2$ for the excited state and $J = 3/2$ for the ground state. These expressions reduce to the corresponding forms for the capture reaction $^7\text{Li}(n, \gamma)^8\text{Li}$ when the long-range Coulomb interaction is turned off [20, 21]. The total cross section and the S -factor can be calculated as

$$\begin{aligned} \sigma(p) &= \frac{1}{16\pi M^2} \frac{1}{2} \left[\frac{p^2 + \gamma_1^2}{2\mu p} |M^{(^2P_{1/2})}|^2 + \frac{p^2 + \gamma_0^2}{2\mu p} |M^{(^2P_{3/2})}|^2 \right], \\ S_{34}(E) &= E e^{2\pi\eta_p} \sigma \left(E = \frac{p^2}{2\mu} \right). \end{aligned} \quad (40)$$

The cross section depends on four unknown parameters related to elastic scattering: s -wave scattering length a_0 and effective range r_0 in the incoming channel, and p -wave effective ranges in the final excited and ground states. These four parameters appear at LO. At NLO, two additional couplings associated with two-body currents appear.

VI. RESULTS AND ANALYSIS

To predict the S -factor at solar energies using the EFT expression in Eq. (40) we need to determine four elastic s - and p -wave scattering parameters, and two couplings for two-body currents. Usually, one-body currents dominate. Thus we start the analysis with the diagrams from Figs. 3 and 4 that can be constrained by elastic scattering, in principle. However, the phase shifts for ${}^3\text{He}(\alpha, \alpha){}^3\text{He}$ are poorly known. The phase shift analysis is from a very old source [31, 32]. Fitting directly to S_{34} measurements is not very constraining. We do a simultaneous fit to S -factor measurements and phase shift analysis to determine the parameters.

The capture data are from LUNA [33], Seattle [34], Weizmann [35], ERNA [36], and Notre Dame [37]. The phase shift data are from Spiger-Tombrello [31] that was analyzed again in Ref. [32] where the experimental errors were quantified. The S_{34} measurements include both prompt photon and activation data. For the former, the branching ratio R_0 to the excited state compared to the ground state is available. The R_0 data are useful as they remove normalization errors from the cross section measurements. We perform three set of fits.

First, we fit the S_{34} , R_0 to c.m. energies of about 500 keV. The s -wave phase shift is fitted to c.m. energies of about 2.7 MeV. We are unable to simultaneously fit to p -wave phase shift and S -factor measurements. It would be preferable to fit the s -wave ERE parameters at lower energies. The available data are only at these higher energies. However, the phase shift data are very smooth so it is possible that the contamination from higher order ERE parameters to the fitted LO a_0 and r_0 is small. Moreover, a fit to only capture data at low energies gives a_0 , r_0 that are compatible with the numbers from simultaneous fit to capture and s -wave scattering data. We call this first fit “Small range” in the plots. Second, we fit the S_{34} , R_0 to c.m. energies of about 1200 keV, and the s -wave phase shift to about 3 MeV. We call this the “Large range” fit in the plots. Finally, we perform a Jackknife fit to the

data. We investigate the errors associated with inter-experimental measurements that might be sensitive to the overall normalization of the capture data. For this, we use the data sets from the “Large range”. The single s -wave phase shift analysis and the branching ration R_0 data are always included. We expect all normalization errors to cancel in R_0 . To perform the Jackknife analysis, we remove one whole dataset from each of the five experimental groups LUNA, Seattle, Weizmann, ERNA and Notre Dame, in turn. The Jackknife value for a certain parameter a is calculated as

$$\begin{aligned}\hat{a} &= N_{\text{group}} a_{\text{global}} - (N_{\text{group}} - 1) \bar{a}, \\ \bar{a} &= \frac{1}{N_{\text{group}}} \sum_{i=1}^{N_{\text{group}}} a_i.\end{aligned}\tag{41}$$

The recipe above removes $\mathcal{O}(1/N_{\text{group}})$ bias from the ordinary Jackknife average for the parameter in question, where a_i ’s are the fit to data after eliminating the i -th group. a_{global} is fit to the entire data set which is the same as the “Large range” fit. $N_{\text{group}} = 5$ for us. The covariance matrix is traditionally calculated from the variance of the individual fits from the average

$$\text{COV}_{ab} = \frac{N_{\text{group}} - 1}{N_{\text{group}}} \sum_{i=1}^{N_{\text{group}}} (a_i - \bar{a})(b_i - \bar{b}).\tag{42}$$

Numerical analyses indicate that both the s -wave scattering length a_0 and effective range r_0 contribute at the same order to the capture amplitude. We propose the following EFT power counting for the ${}^3\text{He}$ - α system based on numerical fits. The low momentum scale is set by $Q \sim \gamma_0 \sim \gamma_1 \sim 60 - 70$ MeV. Assume r_0 is of natural size $\Lambda \sim 1/r_0 \sim 150 - 200$ MeV which is about the pion mass. Then the scattering length has a scaling $a_0 \sim \Lambda/Q^2$ such that in the modified ERE the contributions from both $1/a_0$ and $r_0 p^2/2$ are of similar size for low momenta $p \sim Q$. This scaling behavior for a_0 has been noticed in α - α scattering before [14]. In this power counting, the contribution from initial state strong interaction (Fig. 4) is enhanced by a factor of $1/Q$ over the diagrams without (Fig. 3). The two-body current contribution in Eq. (37) is suppressed by a factor of Q compared to diagrams in Fig. 4, irrespective of the scaling for a_0 , r_0 . We include the two-body current at NLO. The

amplitude from Eq. (37) can then be organized as

$$\begin{aligned}
\mathcal{A}(p) &= \mathcal{A}_{\text{LO}}(p) + \mathcal{A}_{\text{NLO}}(p) + \dots, \\
\mathcal{A}_{\text{LO}}(p) &= \frac{2\pi C_0(\eta_p)e^{i\sigma_0}}{\mu^2} \times \frac{B^{(0)}(p) + \alpha_e B^{(1)}(p) + \Delta B(p) + \mu J_0(p)}{-\frac{1}{a_0} + r_0 p^2/2 - 2k_C H(\eta_p)}, \\
\mathcal{A}_{\text{NLO}}(p) &= -e^{i\sigma_0} \left[\frac{1}{\mu} A(p) + C_0(\eta_p) - \frac{2\pi}{\mu} \frac{C_0(\eta_p)k_0}{-1/a_0 + r_0 p^2/2 - 2k_C H(\eta_p)} \times \frac{L_{E1}^{(\zeta)}}{Z_\phi/m_\phi - Z_\psi/m_\psi} \right].
\end{aligned} \tag{43}$$

In our analysis, we fit the overall wave function renormalization factors $[h^{(\zeta)}]^2 \mathcal{Z}^{(\zeta)}$ for the two p -wave channels instead of the effective range parameters. Higher order corrections to these would include contributions from the shape parameter. However, $[h^{(\zeta)}]^2 \mathcal{Z}^{(\zeta)}$ is a constant, independent of energy, which we simply fit. Thus the theory error in this calculation comes from higher order contributions to the initial state s -wave interaction, recoil effects, and from higher order two-body currents. We estimate the NNLO corrections from the s -wave shape parameter to the diagrams in Fig. 4 to be about Q^2/Λ^2 compared to the LO results. A similar sized error can come from two-body currents beyond what we consider here. We estimate theory error as about Q^2/Λ^2 , i.e. about 10% corrections.

At LO we fit a_0 , r_0 and the two wave function renormalization constants $[h^{(2P_{1/2})}]^2 \mathcal{Z}^{(2P_{1/2})}$, $[h^{(2P_{3/2})}]^2 \mathcal{Z}^{(2P_{3/2})}$. At NLO, we hold a_0 , r_0 , constrained by phase shift analysis [32], fixed. Only the wave function renormalization constants and two-body current couplings $L_{E1}^{(2P_{1/2})}$, $L_{E1}^{(2P_{3/2})}$ are fitted. Fitting all 6 parameters at NLO is possible. This gives similar values to the parameters that we fitted at LO. However, two-body currents are not well constrained and lead to large uncertainty in the wave function renormalization constant. Ideally, the four elastic scattering parameters that enter at LO would be determined from phase shift analysis, and only the two-body currents would need to be fitted to S_{34} measurements at NLO. This is not the case given the lack of quality phase shift data. Constraining only a_0 , r_0 from phase shift data and holding them fixed, leads to better determination of the two-body currents at NLO.

In Table I, we summarize our fits. The four elastic scattering parameters are consistent across the three different kinds of fits: Small range, Large range and Jackknife. This is reflected in the plots in Figs. 6, 7 and 8. The variation in the wave function renormalization from LO to NLO is also within the expected 30% EFT expansion Q/Λ . The two-body currents are not well constrained in the Small range fit. At higher momentum the sensitivity to the two-body currents increases as it has a momentum dependence that scales as $L_{E1}^{(\zeta)}(p^2 +$

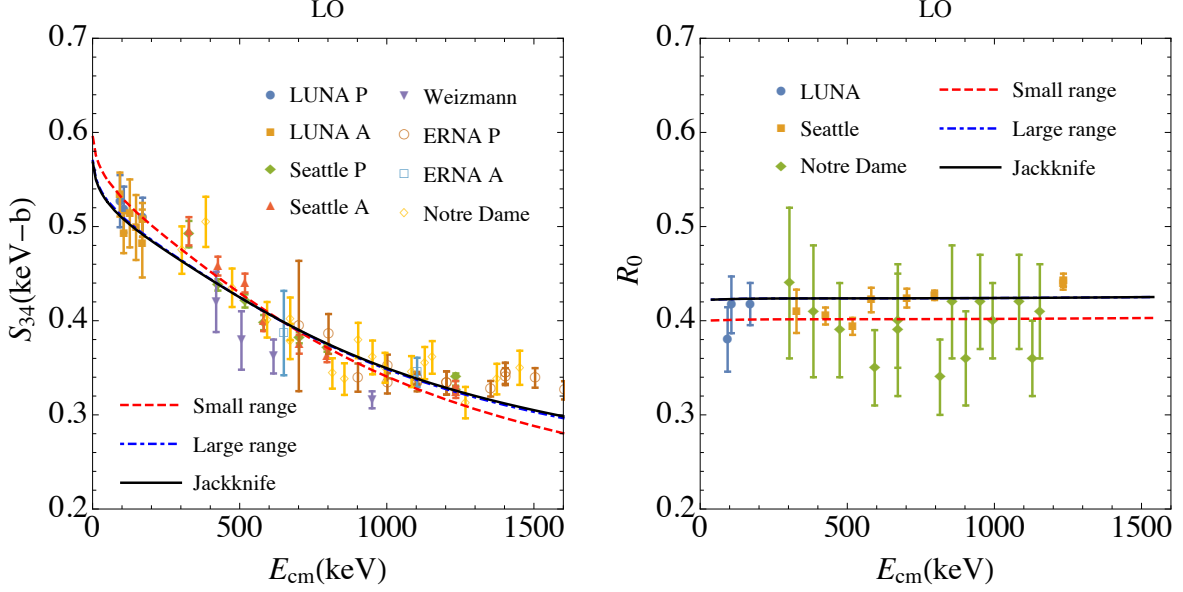


FIG. 6. Radiative capture ${}^3\text{He}(\alpha, \gamma){}^7\text{Be}$ at LO. The left panel shows S_{34} for c.m. energy E_{cm} . The right panel is the ratio of the capture to the excited state over the capture to the ground state. The data are from the references cited in the text. The red dashed, blue dot-dashed and black solid curves are the halo EFT results from three different fits described in the text.

$[\gamma^{(\zeta)}]^2$). The branching ratio plot in Figs. 6, 7 indicates sensitivity to the two-body current. If R_0 increases with energy as suggested by Seattle data, then this trend is captured at NLO where the two-body currents contribute. This could be explored further in the future. Precise measurements of R_0 over a wide range of energy would be useful for such an analysis.

In Table II we list $S_{34}(0)$ in EFT. The errors from the fits were propagated to the S -factor assuming a linear model as follows. For a function $f(\mathbf{r}; \boldsymbol{\beta})$, where \mathbf{r} is the independent variable and $\boldsymbol{\beta}$ the parameter set, we estimate the error as

$$\delta f(\mathbf{r}; \boldsymbol{\beta}) = \sqrt{\frac{\partial f(\mathbf{r}; \boldsymbol{\beta})}{\partial \beta_i} \text{COV}_{ij} \frac{\partial f(\mathbf{r}; \boldsymbol{\beta})}{\partial \beta_j}}. \quad (44)$$

We indicate a theory error of 10% in our estimates. The central values of the EFT fits are higher than other estimates -0.593 FMD [38], 0.59 NCSM [39], $0.567 \pm 0.018 \pm 0.004$ LUNA [33], 0.595 ± 0.018 Seattle [34], $0.53 \pm 0.02 \pm 0.01$ Weizmann [35], 0.57 ± 0.04 ERNA [36], 0.554 ± 0.020 Notre Dame [37]— but they are consistent within the errors.

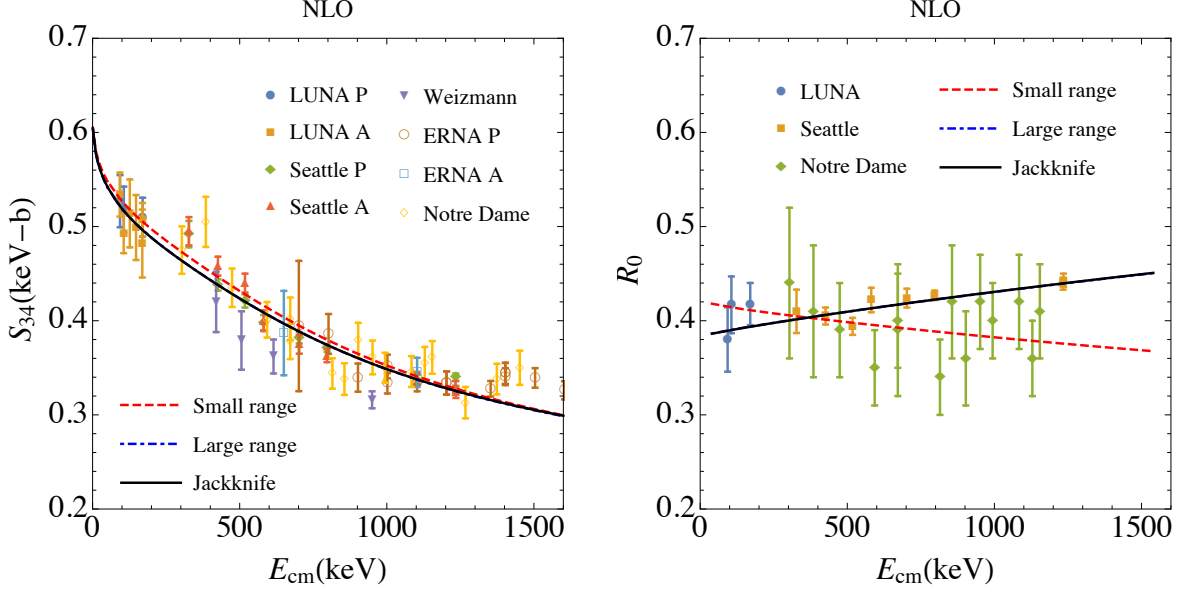


FIG. 7. Radiative capture $^3\text{He}(\alpha, \gamma)^7\text{Be}$ at NLO. The same notations as Fig. 6.

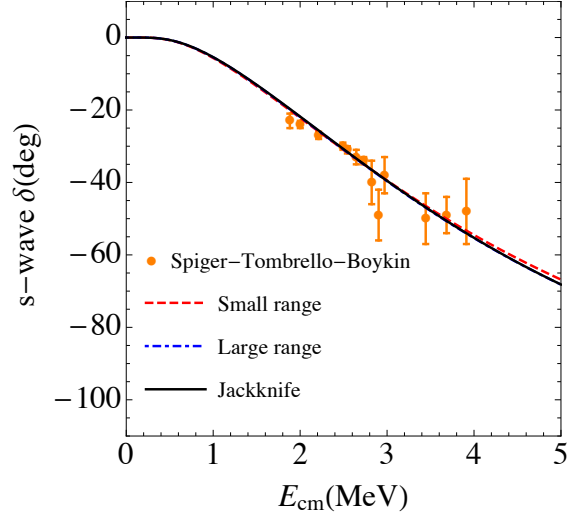


FIG. 8. s -wave phase shift. The data are from the references cited in the text. The red dashed, blue dot-dashed and black solid curves are the halo EFT results from three different fits described in the text.

VII. CONCLUSIONS

The capture cross section σ and the related S -factor S_{34} for $^3\text{He}(\alpha, \gamma)^7\text{Be}$ was calculated at low energies in halo EFT. E1 transitions from initial s -wave state to the bound p -wave

Fits	$a_0(\text{fm})$	$r_0(\text{fm})$	$\mathcal{Z}^{(+)}$	$\mathcal{Z}^{(-)}$	$L_{\text{E1}}^{(+)}$	$L_{\text{E1}}^{(-)}$
Small range (LO)	14.2 ± 0.7	1.31 ± 0.03	0.015 ± 0.001	0.014 ± 0.001	–	–
Small range (NLO)	–	–	0.018 ± 0.001	0.020 ± 0.002	0.3 ± 0.1	0.1 ± 0.1
Large range (LO)	13.2 ± 0.2	1.36 ± 0.01	0.0167 ± 0.0006	0.0165 ± 0.0006	–	–
Large range (NLO)	–	–	0.0239 ± 0.0005	0.0209 ± 0.0006	0.09 ± 0.02	0.24 ± 0.03
Jackknife (LO)	13.1 ± 0.3	1.36 ± 0.01	0.0170 ± 0.0005	0.0168 ± 0.0005	–	–
Jackknife (NLO)	–	–	0.025 ± 0.001	0.022 ± 0.001	0.08 ± 0.02	0.23 ± 0.03

TABLE I. EFT parameters. The parameters were determined from simultaneous fits to the capture ${}^3\text{He}(\alpha, \gamma){}^7\text{Be}$ and s -wave ${}^3\text{He}(\alpha, \alpha){}^3\text{He}$ phase shift data as described in the text. The $L_{\text{E1}}^{(\pm)}$ are the two-body current couplings for capture into the ${}^2P_{3/2}$ and ${}^2P_{1/2}$ bound states, respectively. Similarly $\mathcal{Z}^{(\pm)}$ equals $[h^{(\zeta)}]^2 \mathcal{Z}^{(\zeta)}$ with $\zeta = {}^2P_{3/2}$ and $\zeta = {}^2P_{1/2}$, respectively.

Fit	$S_{34}(0)(\text{keV} \cdot \text{b})$
Present (Small range LO)	0.60 ± 0.01 (fit) ± 0.06 (EFT)
Present (Large range LO)	0.578 ± 0.006 (fit) ± 0.058 (EFT)
Present (Jackknife LO)	0.576 ± 0.007 (fit) ± 0.058 (EFT)
Present (Small range NLO)	0.62 ± 0.07 (fit) ± 0.06 (EFT)
Present (Large range NLO)	0.62 ± 0.03 (fit) ± 0.06 (EFT)
Present (Jackknife NLO)	0.616 ± 0.002 (fit) ± 0.062 (EFT)

TABLE II. S_{34} at threshold. In the EFT results, the first error estimate is from the fits and the second is an estimated 10% error from NNLO corrections. Note that the EFT results are evaluated at $E = 20 \times 10^{-3}$ keV.

ground and excited states were considered. The Coulomb photons between the two clusters ${}^3\text{He}$ and α were iterated to all orders in perturbation. The initial state short-range interaction in the presence of the Coulomb ladder gave the dominant contribution, and constituted the LO amplitude. The EFT expressions were given in terms of four low-energy parameters that were related to ${}^3\text{He}(\alpha, \alpha){}^3\text{He}$ scattering in s - and p -waves, without any model-dependence.

We determine the low-energy parameters by simultaneously fitting the halo EFT expressions to S_{34} measurements and s -wave phase shift. Three different fitting procedures

were employed that gave very similar results. The fits indicate that the s -wave scattering length and effective range both contribute at LO. The contribution from the diagrams without initial state short-range interaction is counted as NLO. The contribution from s -wave shape parameter is suppressed by factor of Q^2/Λ^2 compared to the LO. This constitutes the 10% estimated theory error in the calculation. The two-body current contribution to E1 transition is also estimated to be consistent with this error estimate.

The EFT results were compared with $S_{34}(0)$ model extrapolations of experimental measurements [33–37] and also recent ab initio calculations [38, 39]. The EFT central values are a little higher but consistent with these other estimates (Table II). More precise measurements of elastic scattering ${}^3\text{He}(\alpha, \alpha){}^3\text{He}$ at lower energies would help constrain better the EFT parameters. We find that the available p -wave phase shift analysis [32] is not compatible with the S_{34} measurements. The NCSM calculation of the phase shifts in Ref. [39] also finds discrepancy with the phase shift analysis. The planned TRIUMF experiment to measure phase shifts down to c.m. energies of about 500 keV [40] would be useful to constrain the low-energy theory. It would determine the wave function renormalization constants directly from elastic scattering data without resorting to fits to capture data. The expressions presented here can be directly applied to ${}^3\text{H}(\alpha, \gamma){}^7\text{Li}$ capture calculation where the main difference is the charge $Z_\psi = 1$ of the ${}^3\text{H}$ nucleus. The EFT parameters would have to be tuned to the ${}^3\text{H}-\alpha$ system. This work is under progress. Future work would also include contribution from initial d -wave state which may become noticeable above about 1 MeV.

ACKNOWLEDGMENTS

G.R. thanks the Institute of Physics at University of São Paulo, the Institute for Nuclear Theory at University of Washington, and the Kavli Institute of Theoretical Physics at University of California Santa Barbara for kind hospitality during part of the completion of this research. This work was partially supported by U.S. NSF grants PHY-1307453, PHY-1615092, and FAPESP-2012/50984-4.

-
- [1] R. H. Cyburt and B. Davids, Phys. Rev. **C78**, 064614 (2008).
 - [2] J. N. Bahcall and R. K. Ulrich, Rev. Mod. Phys. **60**, 297 (1988).

- [3] E. G. Adelberger *et al.*, Rev. Mod. Phys. **70**, 1265 (1998).
- [4] S. Fukuda *et al.* (Super-Kamiokande), Phys. Rev. Lett. **86**, 5651 (2001).
- [5] B. Aharmim *et al.* (SNO), Phys. Rev. **C75**, 045502 (2007).
- [6] J. N. Bahcall and A. M. Serenelli, Astrophys. J. **626**, 530 (2005).
- [7] J. N. Bahcall, A. M. Serenelli, and S. Basu, Astrophys. J. **621**, L85 (2005).
- [8] C. Arpesella *et al.* (Borexino), Phys. Rev. Lett. **101**, 091302 (2008).
- [9] R. H. Cyburt, Phys. Rev. **D70**, 023505 (2004).
- [10] B. D. Fields, Ann. Rev. Nucl. Part. Sci. **61**, 47 (2011).
- [11] E. G. Adelberger *et al.*, Rev. Mod. Phys. **83**, 195 (2011).
- [12] C. A. Bertulani, H. W. Hammer, and U. Van Kolck, Nucl. Phys. **A712**, 37 (2002).
- [13] P. F. Bedaque, H. W. Hammer, and U. van Kolck, Phys. Lett. **B569**, 159 (2003).
- [14] R. Higa, H.-W. Hammer, and U. van Kolck, Nucl. Phys. **A809**, 171 (2008).
- [15] B. A. Gelman, Phys. Rev. **C80**, 034005 (2009).
- [16] D. L. Canham and H.-W. Hammer, Eur. Phys. J. **A37**, 367 (2008), 0807.3258.
- [17] D. L. Canham and H.-W. Hammer, Nucl. Phys. **A836**, 275 (2010), 0911.3238.
- [18] V. Lensky and M. C. Birse, Eur. Phys. J. **A47**, 142 (2011).
- [19] H.-W. Hammer and D. Phillips, Nucl. Phys. **A865**, 17 (2011).
- [20] G. Rupak and R. Higa, Phys. Rev. Lett. **106**, 222501 (2011).
- [21] L. Fernando, R. Higa, and G. Rupak, Eur. Phys. J. **A48**, 24 (2012).
- [22] G. Rupak, L. Fernando, and A. Vaghani, Phys. Rev. **C86**, 044608 (2012).
- [23] X. Zhang, K. M. Nollett, and D. R. Phillips, Phys. Rev. **C89**, 024613 (2014).
- [24] X. Zhang, K. M. Nollett, and D. R. Phillips, Phys. Rev. **C89**, 051602 (2014).
- [25] E. Ryberg, F. Christian, H. W. Hammer, and L. Platter, Eur. Phys. J. **A50**, 170 (2014).
- [26] X. Zhang, K. M. Nollett, and D. R. Phillips, Phys. Lett. **B751**, 535 (2015).
- [27] TUNL Nuclear Data Evaluation Project, “*Energy Level Diagram, ^7Be (2002)*”. Available at http://www.tunl.duke.edu/nucldata/figures/07figs/07_04_2002.pdf.
- [28] S. R. Beane and M. J. Savage, Nucl. Phys. **A694**, 511 (2001).
- [29] M. Abramowitz and I. A. Stegun, eds., *Handbook of mathematical functions : with formulas, graphs, and mathematical tables* (Dover, New York, 1965).
- [30] I. J. Thompson, NIST Digital Library of Mathematical Functions, “*Chapter 33: Coulomb Functions*”, <http://dlmf.nist.gov/33>.

- [31] R. J. Spiegel and T. A. Tombrello, Phys. Rev. **163**, 964 (1967).
- [32] W. R. Boykin, S. D. Baker, and D. M. Hardy, Nucl. Phys. A **195**, 241 (1972).
- [33] H. Constantini *et al.*, Nucl. Phys. A **814**, 144 (2008).
- [34] T. A. D. Brown *et al.*, Phys. Rev. C **76**, 055801 (2007).
- [35] B. S. Nara Singh, M. Hass, Y. Nir-El, and G. Haquin, Phys. Rev. Lett. **93**, 262503 (2004).
- [36] A. Di Leva *et al.*, Phys. Rev. Lett **102**, 232502 (2009).
- [37] A. Kontos, E. Uberseder, R. deBoer, J. Grres, C. Akers, A. Best, M. Couder, and M. Wiescher, Phys. Rev. **C87**, 065804 (2013), [Addendum: Phys. Rev.C88,no.1,019906(2013)].
- [38] T. Neff, Phys. Rev. Lett. **106**, 042502 (2011).
- [39] J. Dohet-Eraly *et al.*, Phys. Lett. **B757**, 430 (2016).
- [40] B. Davids, “Elastic scattering of $^3\text{He}+\alpha$ with SONIK,” (2016), private communication.